12th International Conference on Structural Analysis of Historical Constructions
SAHC 2020
P. Roca, L. Pelà and C. Molins (Eds.)

NEW STRATEGIES TO ASSESS THE SAFETY OF UNREINFORCED MASONRY STRUCTURES USING THRUST NETWORK ANALYSIS

R. MAIA AVELINO[1*], A. IANNUZZO[1], T. VAN MELE[1] AND P. BLOCK[1]

[1]Institute of Technology in Architecture (ITA), Block Research Group (BRG)
Eidgenössische Technische Hochschule Zürich (ETH - Zurich)
Stefano-Franscini-Platz 1, HIB E, CH-8093 Zurich, Switzerland
email: {maia, iannuzzo, van.mele, block}@arch.ethz.ch, www.block.arch.ethz.ch
(*corresponding author)

Keywords: Masonry Assessment, Thrust Network Analysis, Optimisation, Equilibrium Analysis, Limit Analysis, Geometric Safety Factor.

Abstract. *This work develops new strategies to robustly apply Thrust Network Analysis (TNA) for the assessment of unreinforced masonry (URM) structures studied within the frame of limit analysis. It formulates and solves a nonlinear optimisation problem on thrust networks considering relevant constraints for the assessment of URM structures. Geometrical and force constraints are include such as the consideration of the structural envelope and bounds on the reaction forces. The objective functions studied correspond to the minimum and maximum horizontal thrusts of the vaults. To evaluate the level of stability of an existing structure, this work develops a methodology to estimate the geometric safety factor (GSF) and the minimum thickness of masonry vaults by solving sequential optimisation problems for increasingly tightened geometrical bounds. This procedure is implemented in a Python-based, open-access tool within the COMPAS framework and illustrated here on two- and three-dimensional applications that are relevant for the structural analysis of historical constructions.*

1 INTRODUCTION

Complex unreinforced masonry vaults present a challenge to engineers and scientists aiming to assess their stability and safety. Historically, since Hooke [1] and Poleni [2], the static approach has been used to assess the stability of masonry construction. Its modern formulation was proposed by Heyman [3] with the establishment of limit analysis of masonry structures. According to the safe theorem of limit analysis, if a path of compressive and equilibrated forces is found within the structural geometry, the structure is safe under the applied loads and this set of compressive, internal forces corresponds to a lower-bound equilibrium solution.

For two-dimensional structures, as classically applied to arches, this internal path reduces to a thrust line [4, 5]. O'Dwyer [6] first extended this concept to the assessment of arcuate masonry vaults by modelling the internal stress states as a discrete network constrained to lie inside the envelope defined by the intrados and extrados of the vault.

Block and Ochsendorf [7] introduced Thrust Network Analysis (TNA), in which the force network is described by its vertical projection in plan, named form diagram, and the equilibrium of the horizontal forces is visualised by a reciprocal graph, named force diagram. As elaborated in [8], TNA is an application of the Force Density Method (FDM) as formulated by Linkwitz

and Schek [9,10]; specifically, in TNA, as applied in this paper, the form diagram is considered fixed. More recent publications extend the optimisation procedure with applications to masonry and analysis of the indeterminacy of the networks [11, 12, 13].

Recently, the methodology was revisited by Marmo and Rosati [14] focusing on the form diagram with the introduction of proportional horizontal loads on the network and by Cercadillo-Garcia and Fernández-Cabo [15] also formulating the problem based on the FDM. Alternatives to thrust networks are presented in Fraternali [16] and Angelillo et al. [17] with polyhedral stress functions and in Fraddosio et al. [18] considering membrane solutions.

Even within the state-of-the art of the different approaches briefly mentioned here, there are still a series of limitations that prevent these methods to be largely adopted in practice. These include the lack of a straightforward methodology to compute the level of stability and/or the (geometric) safety factor for a given vaulted structure, the difficulty to deal with non-proportional horizontal loads, and the lack of flexibility to restrain solutions to geometrical features, such as cracks, hinge lines or openings, and force constraints, such as bounds on the reactions and allowance for horizontal reactions along the perimeter of the vault (open edges).

This paper proposes a computation pipeline to robustly apply TNA for the assessment of unreinforced masonry (URM) vaulted structures by efficiently searching for admissible thrust networks for a given structure. The mathematical formulation is taken from [11, 12], and the search is executed by solving a nonlinear constrained optimisation. In particular, as objective functions, the minimum and the maximum of the horizontal thrust for a given form diagram are considered. The constraints of the optimisation problem are enforced on the geometry (heights of the nodes), on the internal forces (compressive) and on the reactions (limited magnitude and inclination). This paper also provides a direct way to verify the level of stability by computing a lower bound of the geometric safety factor (GSF) of the structure. This is done by iteratively tightening the geometrical envelope of the vault while computing minimum and maximum thrust until the structure reaches its minimum thickness and, at this point, these solutions coincide representing the only possible stress state of the structure, i.e. its limit state.

All analyses are performed with a Python-based, open-access tool. This tool implements TNA [8] and is provided through the COMPAS Masonry framework [19], which is a part of a larger research project that aims to develop appropriate and practical analysis strategies and tools for tackling the assessment of URM structures [19].

The organisation of the paper is as follows. In Section 2, the theoretical background is presented. In Section 3, the computational implementation is described. In Section 4, the new solving algorithm is illustrated with two- and three-dimensional examples. Finally, in Section 5, the findings are summarised, pointing to future research.

2 THEORETICAL BACKGROUND

The safe theorem of limit analysis of masonry structures, proved by Heyman [3], states that if any admissible stress field is found for a given structure, then, the structure is safe under the applied loads. A stress field is admissible if it is equilibrated, compressive and fits entirely within the structural geometry of the masonry. In Angelillo et al. [17], the set of statically admissible stress fields H is described. Thus, according to the safe theorem, if H is not void, any solution found in this set can be accepted as a lower-bound solution for the assessment problem. If H includes only one admissible stress field, the structure is in the so-called limit

state. In existing structures, the concern is how far the current state of the structure, considering the self-weight of the structure and the applied loads, is from the limit state condition. In this paper, we are interested stress fields represented by thrust networks that correspond to singular, one-dimensional stress fields having the forces concentrated on the edges of a network.

2.1 Force Densities in thrust networks

As in the mathematical formulation of [8,11], thrust networks are defined by $n=n_i+n_b$ nodes as the sum of n_i internal nodes and n_b restrained nodes. These nodes are connected by m edges according to a connectivity matrix $\mathbf{C}$. The forces are applied on the internal nodes in any direction as the vectors $\mathbf{p}_x$, $\mathbf{p}_y$, $\mathbf{p}_z$. Linkwitz and Schek [9,10] introduce the force-densities q for an edge, corresponding to the ratio between the force f and the length l of the edge. With $\mathbf{C}_i$ and $\mathbf{C}_b$ the columns sliced from $\mathbf{C}$ corresponding to the internal and restrained nodes of the network. The nodal coordinates are $\mathbf{x}$, $\mathbf{y}$, $\mathbf{z}$ and we consider the relations: $\mathbf{U}=\text{diag}(\mathbf{Cx})$ and $\mathbf{V}=\text{diag}(\mathbf{Cy})$. The horizontal equilibrium of the thrust network becomes:

$$\begin{bmatrix}\mathbf{C}_i^T\mathbf{U}\\ \mathbf{C}_i^T\mathbf{V}\end{bmatrix}\mathbf{q}=\begin{bmatrix}\mathbf{p}_x\\ \mathbf{p}_y\end{bmatrix}. \tag{1}$$

Positive qs represent compression. As in [8, 11], the left-hand side of Eq. (1) is considered in the matrix $\mathbf{E}$ of size ($2n_i$ x m) and the vectors $\mathbf{p}_x$ and $\mathbf{p}_y$ of the applied loads on the internal nodes are stacked in the vector $\mathbf{p}_h$ of size $2n_i$, resulting in the horizontal equilibrium as:

$$\mathbf{Eq}=\mathbf{p}_h. \tag{2}$$

For a fixed form diagram, the matrix $\mathbf{E}$ does not change as it depends only on its connectivity and geometry. Therefore, any set of non-negative $\mathbf{q}$ satisfying Eq. (2) will satisfy horizontal equilibrium for the given/chosen fixed form diagram. For such a $\mathbf{q}$ and given the heights of the restrained nodes $\mathbf{z}_b$, one can compute the heights of free-nodes $\mathbf{z}_i$ as:

$$\mathbf{z}_i=(\mathbf{C}_i^T\mathbf{Q}\mathbf{C}_i)^{-1}\left(\mathbf{p}_z-(\mathbf{C}_i^T\mathbf{Q}\mathbf{C}_b)\mathbf{z}_b\right), \tag{3}$$

with $\mathbf{Q}=\text{diag}(\mathbf{q})$ and the vertical loads $\mathbf{p}_z$, often coming from the self-weight of the masonry.

3 COMPUTATIONAL IMPLEMENTATION

The methodology described in Section 2 allows for the computation of thrust networks. This section describes the computational implementation to automate the search for obtaining thrust networks that are solutions to the problem of assessment of URM structures.

3.1 Force indeterminacy of thrust networks

Computing a non-negative vector $\mathbf{q}$ from Eq. (2) is not an easy task since the equilibrium matrix $\mathbf{E}$, for common topologies, is usually ill-conditioned. For that reason, and also to reduce the number of parameters in the system, the problem can be treated in terms of the independent edges [11,20]. The independent edges are the degrees of freedom of the equilibrium system. Therefore, one can take the force densities assigned to the independent edges $\mathbf{q}_{ind}$ as variables to find the force densities for the rest of the dependent edges $\mathbf{q}_{dep}$ with:

$$\mathbf{q}_{dep}=\mathbf{E}_{dep}^{-1}(\mathbf{p}_h-\mathbf{E}_i\mathbf{q}_{ind}). \tag{4}$$

A possible set of independent edges has its indices related to the columns of the matrix **E** that form a base of linearly independent vectors. Finding a set of columns spanning the rank of the matrix **E** can be done by finding a reduced row-echelon form (RREF) of **E** as in [20].

3.2 Minimum and maximum thrust networks

Following the identification of the degrees of freedom of the network, the general optimisation problem is described in terms of the independent edges ($\mathbf{q}_{\text{ind}}$) and the heights of the restrained nodes ($\mathbf{z}_{\text{b}}$) as follows:

$$\begin{aligned} &\textit{minimise} && f(\mathbf{q}_{\text{ind}}) \\ &\textit{subject to} && c_j(\mathbf{q}_{\text{ind}}, \mathbf{z}_{\text{b}}) \geq \mathbf{0} \\ & && h_k(\mathbf{q}_{\text{ind}}, \mathbf{z}_{\text{b}}) = \mathbf{0} \end{aligned} \quad , \tag{5}$$

in which the equality constraint Eq. (5.3) is Eq. (4), ensuring horizontal equilibrium of the fixed form diagram. The inequality constraints Eq. (5.2) will be discussed in Section 3.3. The objective function can be chosen among a great variety of functions relevant to assessment with thrust networks. This paper will discuss the following ones:

$$\textit{minimise} \qquad f(\mathbf{q}_{\text{ind}}) = \pm \sum_{\text{i}}^{\text{n}_\text{b}} \sqrt{\text{R}_{\text{x,i}}^2 + \text{R}_{\text{y,i}}^2} \ , \tag{6}$$

where $\mathbf{R}_{\text{x}} = \mathbf{C}_{\text{b}}^{\text{T}}\mathbf{Q}\mathbf{C}\mathbf{x}_{\text{b}}$ and $\mathbf{R}_{\text{y}} = \mathbf{C}_{\text{b}}^{\text{T}}\mathbf{Q}\mathbf{C}\mathbf{y}_{\text{b}}$ are the vectors containing the reactions in the x- and y-direction, respectively, for the n_b restrained nodes.

This equation, in its positive form, minimises the horizontal components of the thrust, providing the minimum (or passive) thrust state for the vault, for a given form diagram. Eq. (6) is linear and function of the force densities **q** computed from $\mathbf{q}_{\text{ind}}$ by Eq. (4).

If as objective function we consider the negative form of Eq. (6), we maximise the thrust on the structure, rendering the maximum (or active) thrust state, again for the given form diagram.

In both cases we have to solve a nonlinear constrained optimisation, that is dependent on the starting point. For large problems, it has been found that starting from a compression-only solution improves the convergence of the optimisation even if that initial solution does not fit within the geometry of the masonry. To this end, a minimisation of loadpath as in [21] was used as starting point for the examples in Sections 4.2 and 4.3.

3.3 Geometric and force constraints on thrust networks

The first applied force constraint ensures that the force densities are non-negative. The independent edges ($\mathbf{q}_{\text{ind}}$) have their domain directly restrained to $[q_{min}, q_{max}]$, where q_{min} is 0.0 and q_{max} is a virtual bound sufficiently high to restrain the search space without being activated. The remaining $\mathbf{q}_{\text{dep}}$, calculated from Eq. (4), are constrained from below to be non-negative.

To guarantee that the thrust network is entirely contained within the masonry, all nodes of the thrust network have upper and lower bounds constraints assigned to their z coordinate. These bounds can also be modified to model specific observed failures or cracks on the existing structure, forcing the height of specific nodes of the network to lie in a predefined position. These applications are not studied in this paper but will be treated in a forthcoming paper.

Since the projection of the network remains fixed in plan and the heights of the restrained nodes ($\mathbf{z}_{\text{b}}$) are variables of the optimisation, the computed thrust networks can be completely detached from a given reference datum. This can become an issue for studying a self-standing

semi-circular arch (i.e. with no buttressing or fill). This is addressed by constraining the inclination of the reaction forces such as, when extended, the reaction vector still remains inside the masonry geometry. Such a constraint is illustrated in Sections 4.1 and 4.2.

3.4 Optimisation solvers

The examples presented in this paper were solved with an implementation of the sequential linear-quadratic programming available in the open-source Python package PyOpt [22].

3.5 Limit state for lower-bound solution

The main contribution of this paper is to present a methodology for estimating the limit state (or closeness to collapse) of a given structure by computing its geometric safety factor (GSF). The GSF is defined as the proportion of the total depth (t) of the structure's cross-section to the minimum depth (t') of the offset, tightened cross-section required to contain a thrust line [23], or in our case, a thrust network. The procedure developed to obtain the GSF sequentially solves the optimisation for maximum and minimum thrust for a decreasing thickness until the respective results coincide. This condition represents the limit state of the structure, since only one stress state is possible, that is, only one thrust line or network (for a given form diagram) fits in the geometry. At this point, the minimum thickness t', and the GSF = t/t' are computed.

4 NUMERICAL APPLICATIONS

Three applications to URM structures are investigated. First, a semi-circular arch (Section 4.1) is analysed, followed by a dome (Section 4.2) and a rectangular cross vault (Section 4.3).

4.1 Semi-circular arch

The first application looks at a semi-circular arch with base geometry described by a central radius R=1.00m and thickness t=0.20m, i.e. t/R=0.20. The linear form diagram is discretised in 20 nodes equally spaced with regards to the projection onto the circular geometry. The out-of-plane dimension of the arch is 1.00m and the density of the masonry ρ=20kN/m^3. The self-weight is lumped at the nodes. The total vertical loading is W=12.6kN. This problem has three variables: one independent ($\mathbf{q}_{ind}$) and the height of the two restrained nodes ($\mathbf{z}_b$). Eq. (6) is used to find the minimum and maximum thrust on the arch depicted on Figure 1a and b, respectively.

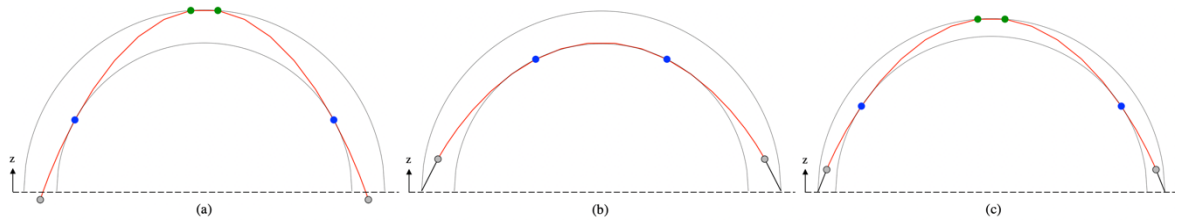

Figure 1: Solutions of minimum (a) and maximum (b) thrust for the semi-circular arch with t/R=0.20 and thrust for the minimum thickness (c) calculated as t'/R=0.1079 after incremental reduction of the thickness.

For the initial configuration t/R=0.20, the ratios of the minimum and maximum thrusts over the self-weight are $(T/W)_{min}$=31.6% and $(T/W)_{max}$=51.2%. The points where the thrust line

touches the intrados and extrados are highlighted in blue and green and the boundary nodes are shown in grey. The segments of the thrust line are depicted in red and the reaction vector is displayed in black when the restrained node is above the reference surface of height z=0.0m. In the solution for the minimum thrust, the restrained nodes go below the reference surface and for the maximum, the restrained nodes go above it and the resultant of the forces touch exactly the extrados of the semi-circular arch (Figure 1b).

Figure 2 visualises the sequential GSF procedure for this example. The optimisation for maximum and minimum is performed reducing t by increments of -0.005m until t=0.110m, and -0.001m afterwards. For each new thickness, minimum and maximum thrust are plotted in Figure 2 until they coincide, representing the limit state where only one thrust line is possible.

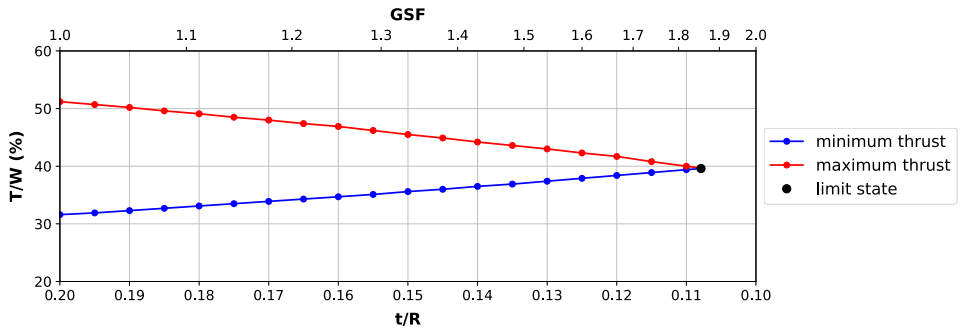

Figure 2. Methodology for deriving the minimum thickness and computing the geometric safety factor (GSF) for the semi-circular arch with t/R=0.20, resulting in t'/R=0.1079 and GSF=1.85.

The minimum thickness t' (or its adimensional t'/R) of the semi-circular arch can be derived as the intersection of the two lines of Figure 2, where we find t'/R=0.1079 and $(T/W)_{limit}$=39.7%. It is known from [5] that the analytical solution for this problem is $(t/R)_{theory}$=0.1075. The error of the proposed methodology is 0.4%, for the discretisation adopted (20 nodes). From this, the GSF can be approximated as the ratio between t and t', resulting in GSF=1.85 (Figure 2).

4.2 Hemispherical dome

For three-dimensional analysis, the assumptions on the force pattern for the masonry vaults become critical. Since the form diagram remains fixed, it should include a logic related to the way that the compressive forces flow to the supports, as in [12]. Therefore, we study two form diagrams to assess a circular dome with a central radius of R=5.0m and thickness t=0.50m, i.e. t/R=0.10 (Figure 3a) under self-weight. The first diagram presents a radial arrangement of the forces to the support; it is composed of 20 meridians and seven circular hoops. As in Section 4.1, the hoops are equally spaced with regards to the base surface and not with the planar projection (Figure 3b). The second form diagram assumes a spiralling force flow (Figure 3c). Both diagrams are composed of 320 edges, have 25 and 18 independent edges respectively that are highlighted in Figure 3. Supports are assigned on the perimeter. The self-weight is assigned according to the 3D tributary area with regards to its projection on the base surface, its thickness t and density ρ=20kN/m^3. The total weight is W=1570kN.

The result for both patterns regarding minimum, maximum thrust and limit thickness are depicted in Figures 4 and 5. Branches with null compressive force are not shown and the

compressive branches have their thickness proportional to the force carried. The points touching the intrados and extrados are marked with blue and green spheres. The same incremental analysis for reduced values of thickness is conducted and the results are plotted in Figure 6.

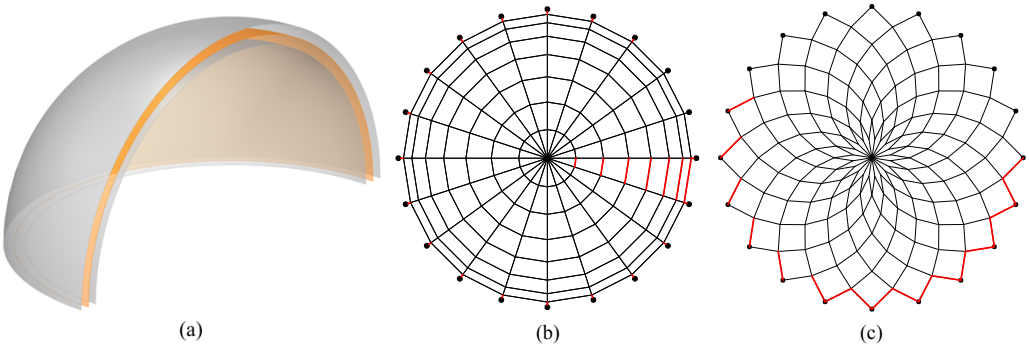

Figure 3. (a) Geometry of the dome with t/R=0.10, showing base surface (orange), intrados and extrados (cut to enhance visualisation); (b) radial form diagram and; (c) spiral form diagram showing independent edges.

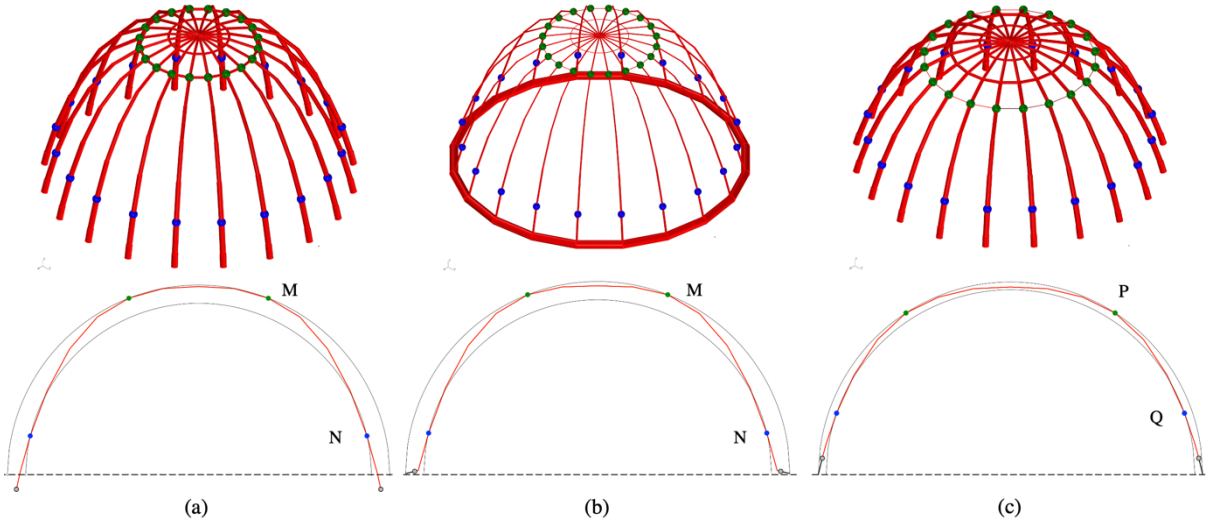

Figure 4. Minimum (a) and maximum (b) thrust solutions for the dome with the radial diagram with t/R=0.10 and with limit thickness (c) achieved (t'/R=0.041). Maximum forces in the plots are 70; 1000; and 72kN.

In the radial diagram, minimum and maximum thrust-over-total-weight ratios for t/R=0.10 are $(T/W)_{min}$=19.8% and $(T/W)_{max}$=430% (Figures 4a-b). The minimum thickness calculated with the radial diagram is t'/R=0.041 where the thrust achieved is $(T/W)_{limit}$=24.4% (Figure 4c). With this result, the safety factor for the dome is estimated as GSF_1=2.42 (Figure 6).

The minimum thrust solution (Figure 4a) shows a bi-axial compressive cap in the upper portion of the dome and an uni-axial stress state towards the supports, where null hoop forces are observed. Looking at a section, the thrust touches the extrados in points M (extrados) and N (intrados) (Figure 4a). Such a stress field is compatible with Heyman's 'orange-slice' mechanism proposed in [23] for an outward (passive) radial displacement of the supports. In this mechanism, cracks form along the meridians where the hoop forces are null and a top cap is preserved uncracked. One can see that while in two dimensions (Section 4.1), the points

touching the intrados and extrados are the only information about cracks (or mechanisms), in the dome, null-forces give additional information about kinematics on the structure.

For the maximum thrust solution (Figure 4b), a compressive ring with high forces is activated in the base of the dome while the magnitude of the forces in the rest of the dome is inferior (see thicknesses of edges). The touchpoints remain in M and N. This suggests that under inward (active) displacement of the supports, a global mechanism for the dome is not activated and the stability is ensured by the compressive ring in the base. This ring creates a discontinuity on the thrust as depicted in the section (Figure 4b), that redirects the reaction force to become almost horizontal. The high difference between maximum and minimum thrust values (22 times greater) gives an idea of the magnitude of the radial pressure supported by the dome.

For the dome in limit thickness condition (Figure 4c) the section and force flow are similar to the minimum thrust with a larger bi-axial cap and section touching in points P (extrados) and Q (intrados). The minimum thickness calculated for the radial diagram is similar to the theoretical $(t/R)_{theory}$=0.042, from [23], with error of 1.4%.

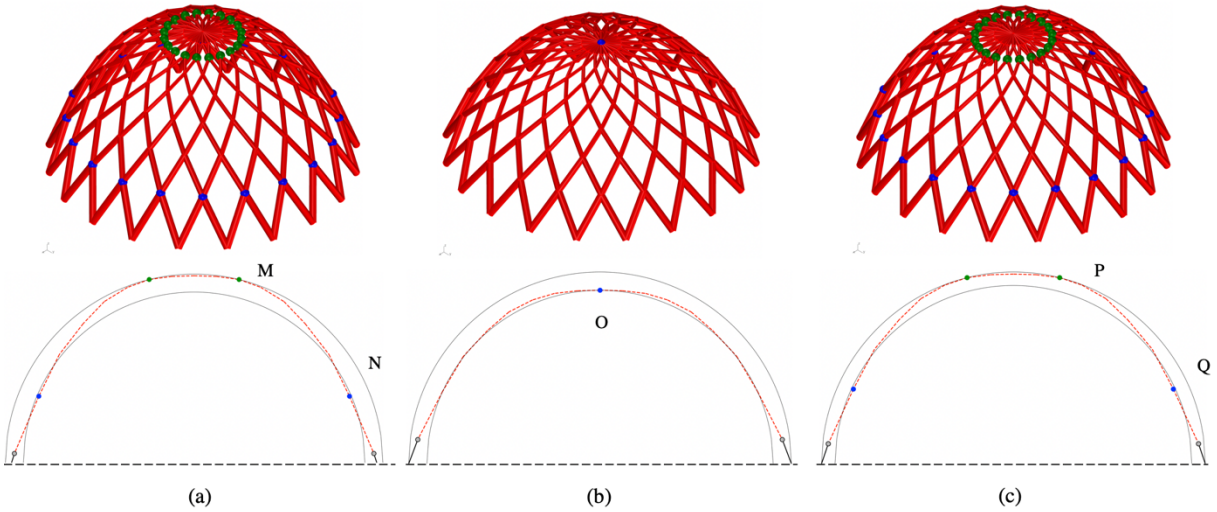

Figure 5. Minimum (a) and maximum (b) thrust solutions for the dome with the spiral diagram with t/R=0.10 and with limit thickness (c) achieved (t'/R=0.073). Maximum forces in the plots are 33; 35; and 34kN.

In the spiral diagram, the minimum and maximum thrust-over-total-weight ratios for t/R=0.10 calculated are $(T/W)_{min}$=31.3% and $(T/W)_{max}$=37.9% (Figure 5a-b). The minimum thickness calculated for this diagram is t'/R=0.073 , with $(T/W)_{limit}$=33.7% (Figure 5c). Such results allow the computation of the safety factor GSF_2=1.37 (Figure 6).

In the spiral diagram, due to its topology, null-force hoops cannot happen; as a consequence, the form diagram will always represent an uncracked solution that does not allow for the 'orange-sliced' mechanism. The GSF_2 found for this pattern is lower, and thus more/over conservative, than for the radial diagram GSF_1. This difference shows the importance of the choice of the form diagram for the assessment with thrust networks. One can also observe that the diagram better aligned with the known pathologies of a dome (radial diagram) resulted in a higher factor of safety and in a further limit state (Figure 6). As expected, refining the diagrams would reduce the errors in the analysis with networks resulting in a slightly higher minimum thickness. However, a sensitivity study on the number of edges is out of the scope of this paper.

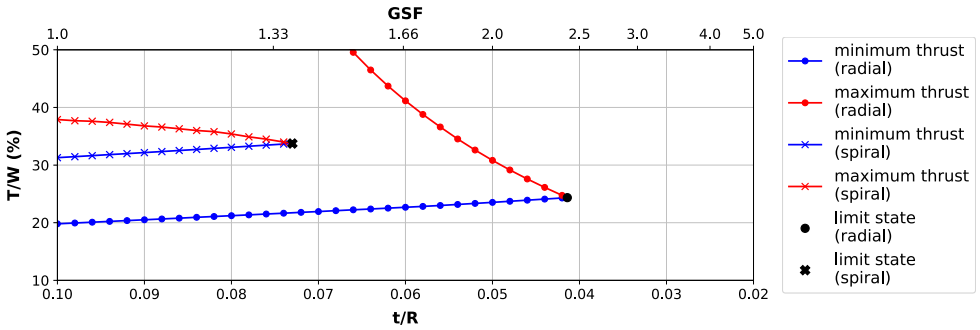

Figure 6. Methodology for deriving the minimum thickness and computing the GSF for the dome (t/R=0.10), the radial diagram resulted in t'/R=0.036 and GSF_1=2.42 and the spiral diagram in t'/R=0.073 and GSF_2=1.37. (Values of T/W higher than 50% not shown for clarity).

4.3 Rectangular cross-vault

We replicate the same analysis for a rectangular rounded cross vault with dimensions 10.0x7.5m and a thickness of t=0.50m. The adimensional parameter is taken with regards to the larger span as t/R=0.10. The geometry is defined by the intersection of two cylinders, the smaller becoming an ellipse. This base geometry is depicted in orange (Figure 7a), with the intrados and extrados for t. Two patterns are proposed referred to as cross- and fan-diagram (Figures 7b-c). The first presents an orthogonal path to the diagonals and then via the groins to the supports, while the second, connects the mid-span to the supports in a straight fashion. The cross diagram has 884 edges, 19 independent edges and the fan has 1024 edges, 36 of which are independent. The self-weight is lumped in the nodes according to the 3D tributary area regarding the projection of the diagrams in the base surface resulting in a total W=902kN for ρ=20kN/m^3. We consider only the four corners of the form diagram to be supported. The results for both patterns regarding minimum, maximum thrust and limit thickness are depicted in Figures 8 and 9. The same incremental analysis is conducted as depicted in Figure 10.

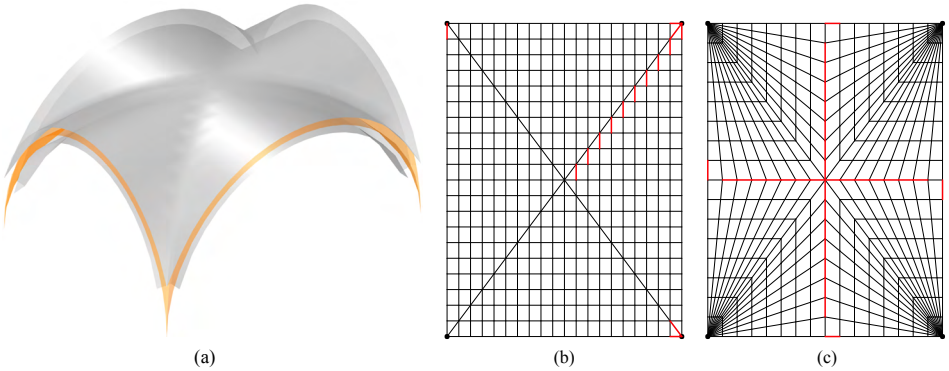

Figure 7. (a) Geometry considered for the rectangular cross-vault (t/R=0.10) , showing base surface (orange), intrados and extrados; (b) cross form diagram and; (c) fan form diagram showing the independent edges.

The adimensional minimum and maximum thrust for the cross diagram are $(T/W)_{min}$=67.5% and $(T/W)_{max}$=96.7% for the initial case t/R=0.10. The minimum thickness calculated in the cross diagram is found to be t'/R=0.061, for a thrust of $(T/W)_{limit}$=76.9%. For the fan diagram,

the difference between the minimum and maximum thrust for t/R=0.10 is smaller, as the optimisation resulted in $(T/W)_{min}$=75.4% and $(T/W)_{max}$=90.9%. The limit state is found for t'/R=0.084, corresponding to a thrust of $(T/W)_{limit}$=80.7%. Based on these values, one can find an estimate to the GSF of the rectangular cross vault studied as GSF_1=1.64 for the cross diagram and GSF_2=1.20 for the fan diagram (Figure 10). This again significant difference, as in the dome example, reaffirms the importance of the form diagram to the present methodology.

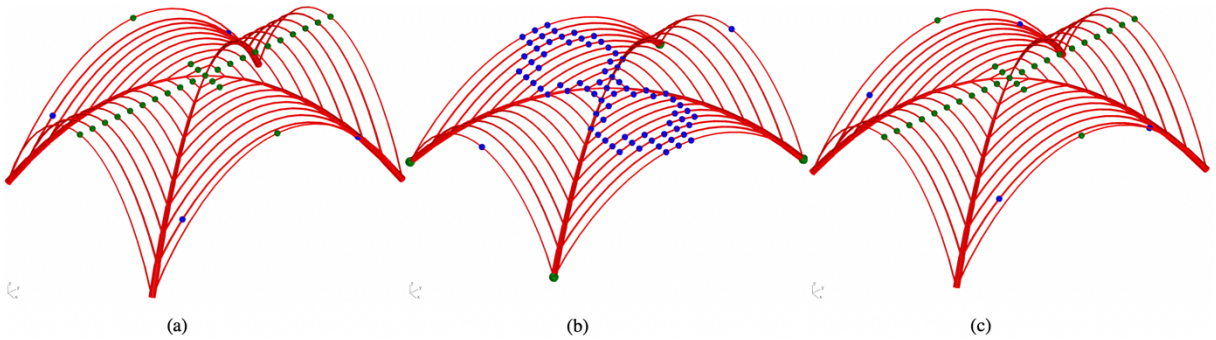

Figure 8. Cross form diagram: minimum (a) and maximum (b) thrust result for t/R=0.10 and thrust for minimum thickness (c) achieved with grid diagram with t'/R=0.061. Maximum forces in plots are 203; 226; and 213kN.

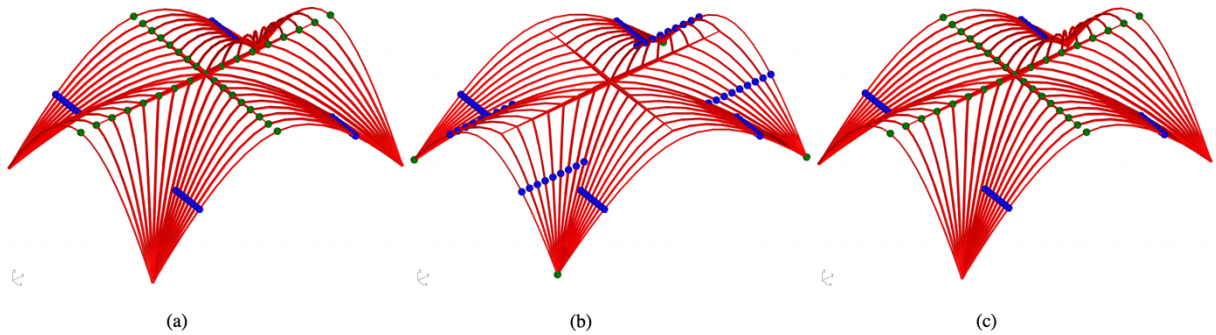

Figure 9. Cross form diagram: minimum (a) and maximum (b) thrust result for t/R=0.10 and thrust for minimum thickness (c) achieved with fan diagram with t'/R=0.084. Maximum forces in plots are 68; 84; and 72kN.

For both diagrams, the minimum thrust touches the extrados in the central portion of the nave, along both spans (Figure 8a and 9a). For the cross diagram, this is more evident in the direction of maximum span (Figure 8a). In the maximum thrust solution, the shallowest thrust is found, which is evident since the network touches the intrados in several points (Figure 8b). For the fan diagram, however, it is observed that the same problem of maximisation did not present such a high number of touching points. Another important difference between the patterns is the fact that for the cross diagram, the forces accumulate along the diagonals, while in the fan diagram, the forces are distributed and the compression force accumulate along the ridges towards the central portion of the vault (Figures 8 and 9).

Regarding the limit analysis, the cross diagram achieved a higher safety factor GSF_1=1.64 against GSF_2=1.20. Similarly to the dome example, the best performing (or less conservative) pattern (i.e. the one with higher GSF) can be seen as a better approximation of the common crack pattern found on cross vaults, known as Sabouret cracks [23] that run parallel to the perimeter of the structure (open edges).

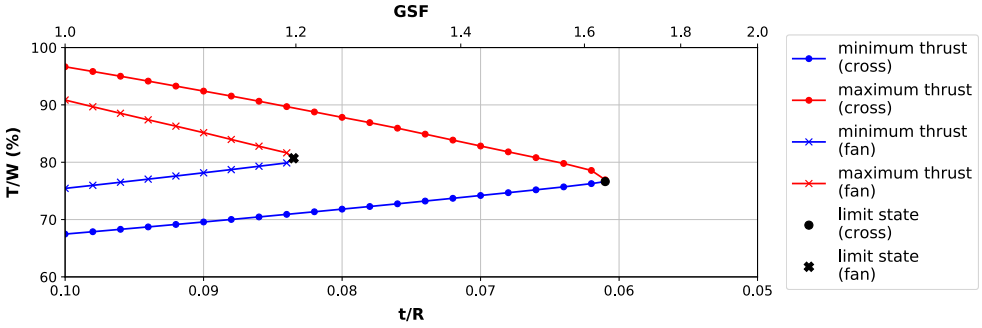

Figure 10. Methodology for deriving the minimum thickness and computing the GSF for the cross vault, cross diagram resulted in t'/R=0.061 and GSF_1=1.64 and the fan diagram in t'/R=0.084 and GSF_2=1.20.

5 CONCLUSION

In the present paper, a methodology to assess masonry structures under vertical loading with thrust networks is developed and implemented in a Python-based tool. A network is described by its fixed projection in plan, the values of its independent force densities $\mathbf{q}_{ind}$ and the heights of the restrained boundary nodes $\mathbf{z}_b$. A nonlinear constrained optimization, with variables $\mathbf{q}_{ind}$ and $\mathbf{z}_b$, is performed yielding the minimum and maximum thrust states for a given masonry vault and form diagram. By sequentially solving for the minimum and maximum thrust networks for decreasing thickness, a methodology for computing the geometric safety factor (GSF) is developed allowing to estimate the closeness to collapse of a given structure. Three applications have been shown: a semi-circular arch, a dome and a cross vault.

A key advantage of the present formulation lies in the fact that it can assess the structure taking as input only the geometry of the intrados and extrados of the vault. On the other hand, the method is built on the formulation of the independent edges, so the solution will be dependent on the given form diagram that cannot change during iterations. This form diagram should be chosen carefully based on assumptions of the flow of forces of the structure to assess. Indeed, it was observed that patterns representing a better approximation of the common crack patterns observed in masonry vaults resulted in higher values of GSF.

Even if not explicitly shown in the examples, the methodology can be extended to estimate the load-bearing capacity under application of additional vertical and horizontal loads. Further development will focus on identifying adapted form diagrams to each problem as even in the presence of an initial, non-perfect (cracked) configuration.

Acknowledgements. This work was supported by the Swiss National Science Foundation (SNSF) - project grant #178953: “Practical Stability Assessment Strategies for Vaulted Unreinforced Masonry Structures”.

REFERENCES

[1] Hooke, R. *A description of helioscopes, and some other instruments*. London: printed by T.R. for John Martyn, (1676).

[2] Poleni, G. *Memorie istoriche della gran cupola del Tempio Vaticano*. Padua: Stamperia del Seminario, (1748).

[3] Heyman, J. The stone skeleton. *Int. J. Solids Struct* (1996) **2(2)**:249-279.

[4] Huerta, S. Mechanics of masonry vaults: The equilibrium approach. In: *3rd Int. Semin. Hist. Constr. Guimarães, Port.* (2001), pp. 47-70.
[5] Ochsendorf, J. Collapse of masonry structures. University of Cambridge, (2002).
[6] O'Dwyer, D. Funicular analysis of masonry vaults. *Comput. Struct.* (1999) **73**:187-197.
[7] Block, P. and Ochesendorf, J. Thrust network analysis: A new methodology for 3D equilibrium. *J. Int. Assoc. Shell Spat. Struct.* (2007) **48(155)**:1-7.
[8] Block, P. Thrust Network Analysis. Massachusetts Institute of Technology, (2009).
[9] Linkwitz K. and Schek, H. Einige Bemerkungen zur Berechnung von vorgespannten Seilnetzkonstruktionen. *Ing. Arch*. (1971) **40**:145-158.
[10] Schek, H. The force density method for form finding and computation of general networks. *Comput. Methods Appl. Mech. Eng.* (1974) **3**:115-134.
[11] Block P. and Lachauer L. Three-dimensional funicular analysis of masonry vaults. *Mech. Res. Commun.* (2014) **56**:53-60.
[12] Block P. and Lachauer, L. Three-dimensional (3D) equilibrium analysis of gothic masonry vaults. *Int. J. Archit. Herit.* (2014) **8(3)**:312-335.
[13] Van Mele, T., Panozzo, D., Sorkine-Hornung, O. and Block, P. Best-fit thrust network analysis: Rationalization of freeform meshes. In: *Shell Structuctures for Archiecture - Form Finding and Optimization*, Routledge (2014), pp. 157-169.
[14] Marmo, F. and Rosati, L. Reformulation and extension of the thrust network analysis. *Comput. Struct.* (2017) **182**:104-118.
[15] Cercadillo-García C. and Fernández-Cabo, J. L. Analytical and Numerical funicular analysis by means of the Parametric Force Density Method. *J. Appl. Res. Technol.* (2016) **14(2)**:108-124.
[16] Fraternali, F. A thrust network approach to the equilibrium problem of unreinforced masonry vaults via polyhedral stress functions. *Mech. Res. Commun.* (2010) **37(2)**:198-204.
[17] Angelillo, M., Babilio, E. and Fortunato, A. Singular stress fields for masonry-like vaults. *Contin. Mech. Thermodyn.* (2013) **25(2)**:423-441.
[18] Fraddosio, A., Lepore, N. and Piccioni, M. D. Thrust Surface Method: An innovative approach for the three-dimensional lower bound Limit Analysis of masonry vaults. *Eng. Struct.* (2019) **202**:109846.
[19] Iannuzzo, A., Dell'Endice, A., Maia Avelino, R., Kao, G.T.C., Van Mele, T. and Block, P. COMPAS Masonry: A Computational Framework for Practical Assessment of Unreinforced Masonry Structures. In: *Proceedings of the SAHC Symposium*, Barcelona, (2021).
[20] Van Mele T. and Block P. Algebraic graph statics. *CAD Comput. Aided Des.* (2014) **53**:104-116.
[21] Liew, A., Avelino, R., Moosavi, V., Van Mele, T. and Block, P. Optimising the load path of compression-only thrust networks through independent sets. *Struct. Multidiscip. Optim.* (2019) **60(1)**:231-244.
[22] Perez, R. E., Jansen, P. W. and Martins, J. R. R. A. pyOpt: A Python-Based Object-Oriented Framework for Nonlinear Constrained Optimization. *Struct. Multidiscip. Optim.* (2012) **45(1)**:101-118.
[23] Heyman, J. *The Stone Skeleton: Structural Engineering of Masonry Architecture*. Cambridge University Press, (1995).